Novel compound heterozygous *CNGA3* mutation associated with retinal cone dystrophy

RUI SUN[1,2*], YAO WANG[1,2*], WENTAO ZHOU[1,2], SHUJIAN CHEN[1,2], YAFEI LI[2], MENG PAN[1,2], DANDAN JI[2], JIN LI[1,2] and XUEFENG SHI[1]

[1]Tianjin Key Laboratory of Ophthalmology and Visual Science, Tianjin Eye Institute, Tianjin Eye Hospital, Clinical College of Ophthalmology, Tianjin Medical University, Tianjin 300020, P.R. China; [2]Department of Cell Biology, The Province and Ministry Co-sponsored Collaborative Innovation Center for Medical Epigenetics, School of Basic Medical Sciences, Tianjin Medical University, Tianjin 300070, P.R. China

Received July 10, 2024; Accepted April 4, 2025

DOI: 10.3892/etm.2025.12905

Abstract. Retinal cone dystrophy (COD) is an inherited retinal disease characterized by reduced central vision, color vision defects and photophobia, resulting from the degeneration of photoreceptors in cone cells, and commonly occurs due to mutations in cyclic nucleotide-gated channel subunit α 3 (*CNGA3*). *CNGA3* mutations are associated exclusively with autosomal recessive retinal disorders, requiring homozygous or compound heterozygous mutations for pathogenicity. In the present study, whole-exome sequencing was performed on a 9-year-old girl diagnosed with COD and her parents, which identified a compound heterozygous *CNGA3* mutation in the proband. The previously reported c.C1001T:p.S334F variant was inherited from her mother and a novel frameshift mutation, c.566_567insT:p.R189fs, was inherited from her father. Further analysis identified that the p.S334F mutation affects a conserved residue in the ion-transport (ion-trans) structural domain, while the frameshift mutation p.R189fs introduces a premature stop codon at position 194, resulting in a truncated protein that retains only the ion-trans structural domain and lacks the cysteine-rich CAP domain-extended domain and cyclic nucleotide-gated ligand-binding zinc finger-like domain. Through ectopic expression in 293T cells and western blotting, p.S334F mutated *CNGA3* was observed to increase CNGA3 protein levels, while the p.R189fs mutation produced a truncated protein. These findings suggest that both mutations compromise normal CNGA3 channel function and are likely to contribute to the disease pathogenesis.

Correspondence to: Professor Xuefeng Shi, Tianjin Key Laboratory of Ophthalmology and Visual Science, Tianjin Eye Institute, Tianjin Eye Hospital, Clinical College of Ophthalmology, Tianjin Medical University, 4 Gansu Road, Heping, Tianjin 300020, P.R. China
E-mail: shixf_tmu@163.com

Professor Jin Li, Department of Cell Biology, The Province and Ministry Co-sponsored Collaborative Innovation Center for Medical Epigenetics, School of Basic Medical Sciences, Tianjin Medical University, 22 Qixiangtai Road, Heping, Tianjin 300070, P.R. China
E-mail: jli01@tmu.edu.cn

*Contributed equally

Key words: CNGA3, retinal cone dystrophy, whole-exome sequencing, genetic variants, hereditary disease

Introduction

Retinal cone dystrophy (COD) is a heterogeneous inherited retinal disease with a prevalence of 1 in 30,000-40,000 individuals (1). The disease is characterized by decreased central vision, color vision impairment and increased sensitivity to light, due to abnormal photoreceptor function in early-stage retinal cone cells. As the disease progresses, the photoreceptor function of rods deteriorates, resulting in night blindness and loss of peripheral vision. COD can be classified as stable or progressive. The stable form presents with congenital or early infantile onset, which is primarily characterized by cone cell dysfunction, whereas the progressive type presents with later onset, typically in mid-adolescence or later, and progressively involves rod photoreceptors (2).

Cyclic nucleotide-gated channel subunit α 3 (*CNGA3*), located on chromosome 2q11.2, encodes a member of the CNG cation-channel protein family that is crucial for normal vision (3). *CNGA3* mutations are associated with color vision disorders, including color blindness (4), and even cone cell dystrophy and Leber congenital amaurosis in rare cases (5). To date, 36 *CNGA3* mutations have been associated with cone cell dystrophy and 102 have been associated with color blindness recorded in the Human Gene Mutation Database (https://www.hgmd.cf.ac.uk/ac/index.php).

The present study reports a case of COD in a young girl exhibiting bilateral reduced visual acuity and mild nystagmus. Whole-exome sequencing was performed on the proband and the unaffected parents, followed by bioinformatic filtering of rare variants and validation via Sanger sequencing. Identified *CNGA3* mutations were cloned into expression plasmids, transfected into 293T cells and analyzed by western blotting. The protein stability and tissue expression patterns were assessed

by bioinformatics tools. The findings expand the *CNGA3* mutation spectrum in COD pathogenesis and suggest that specific *CNGA3* structural domains may represent mutation hotspots in COD, highlighting potential targets for developing therapies for *CNGA3*-related retinal diseases.

Materials and methods

Sample collection and whole-exome sequencing. Peripheral blood was obtained from the patient, a 9-year-old girl with COD, in September 2020 at Tianjin Eye Hospital (Tianjin, China). During the same hospital visit, peripheral blood samples were also collected from the parents, who had not been diagnosed with any associated eye disease. The patient underwent eye examinations, including fundus photography, optical coherence tomography (OCT) and electroretinography (ERG). Follow-up was performed once yearly.

High-throughput sequencing of the samples was performed by Novogene Co., Ltd. DNA libraries were prepared for sequencing using the NEBNext® Ultra™ DNA Library Prep Kit (E7370L; New England Biolabs, Inc.). The quality of the samples was verified by the 5400 Fragment Analyzer System (Agilent Technologies Inc.). Exome sequencing was performed using an NovaSeq 6000 Sequencing System (Illumina, Inc.) using paired-end 150-bp reads. The NovaSeq 6000 S4 Reagent Kit v1.5 (Illumina, Inc.) was used for sequencing. Library concentrations were assessed using the CFX96 Touch Real-Time PCR Detection System (Bio-Rad Laboratories Co., Ltd.) and an Invitrogen Qubit 4 Fluorometer (Thermo Fisher Scientific, Inc.).

Whole exome sequencing data analysis. The data files obtained from high-throughput sequencing were analyzed by Base Calling and converted into Sequenced Reads, and then sequencing data were aligned with the human reference genome (Genome Reference Consortium Human Build 37) using BWA (version 0.7.8-r455; https://github.com/). Variant calling was performed using SAMtools (version 1.21) (6) and the resulting VCF files were annotated using ANNOVAR (version 2022-01-13) (7).

Pathogenic variants were screened based on the following criteria: i) Variants with an allele frequency of <1% in the 1000 Genomes (8) Exome Sequencing Project 6500 (https://www.ebi.ac.uk/ena), Genome Aggregation databases (9) and ChinaMap (http://www.mbiobank.com/) were retained; ii) only variants located in the coding (exonic) or in the splice site (±10 bp) regions were retained; iii) nonsynonymous mutations in highly conserved regions (grep++ score >2) and those affecting splicing (dbscSNV score >0.6) were retained, whereas small (<10 bp) fragments of non-displaced indel mutations located in the repeat region were excluded; iv) variants predicted to be deleterious using two of the following four functional annotation algorithms were retained: Sorting Intolerant from Tolerant (SIFT) (10), Polymorphism Phenotyping v2 (PolyPhen-2) high-diversity model (11), MutationTaster (12) and Combined Annotation Dependent Depletion (13); and v) alignment with autosomal recessive or compound heterozygous inheritance patterns.

Molecular cloning and Sanger sequencing. Genomic DNA was extracted from peripheral blood samples using the Magnetic Blood DNA Extraction Kit (Vazyme Biotech Co., Ltd.) and primers were designed using Primer3 (https://primer3.org/). The primer sequences are listed in Table SI.

To analyze the mutant allele c.566_567insT:p.R189fs, PCR was performed to amplify the target locus. The thermal cycling protocol consisted of initial denaturation at 95˚C for 5 min, followed by 35 cycles of denaturation at 95˚C for 30 sec, annealing at 57˚C for 4 min and extension at 72˚C for 4 min. The resulting PCR products were cloned into the pEASY-Blunt Zero Cloning vector and transformed into *Trans*1-T1 receptor cells using the pEASY-Blunt Zero Cloning Kit (TransGen Biotech Co., Ltd.) following the manufacturer's instructions. Sanger sequencing was performed on individual clones using M13 forward and reverse primers to confirm the presence of the mutation in the patient samples.

CNGA3 plasmid construction. The pcDNA3.1 plasmid containing the *CNGA3* cDNA sequence (Table SII) with a C-terminal FLAG tag (Table SIII) was synthesized by Beijing Tsingke Biotech Co., Ltd. The *CNGA3* sequence in the National Center for Biotechnology Information database (accession number, NM_001298.3) was used. This matched the sequences of the alleles from the father and mother of the proband, confirming they carried wild-type alleles. The *CNGA3* wild-type plasmid was designated pcDNA3.1-CNGA3 (Fig. S1).

To introduce a p.S334F mutation, the Mut Express II Fast Mutagenesis Kit V2 (Vazyme Biotech Co., Ltd.) was used. The pcDNA3.1-CNGA3-p.S334F (c.C1001T) mutant plasmid was generated using pcDNA3.1-CNGA3 as a template. Mutation-specific primers were designed as follows: Forward primer (p.S334F-F): 5'-GACAGACTtCTGGGTCTACCCAAACATCTCAA-3' (plasmid positions, 1,984-2,015), which corresponds to bases 993-1,024 in the *CNGA3* coding sequence (CDS), with the lower case 't' indicating the mutation site between bases 1,000 and 1,002; and reverse primer (p.S334F-R): 5'-AGACCCAGaAGTCTGTCCCAAACCAATGAACT-3' (plasmid positions, 1,968-2,000), which corresponds to the reverse complementary sequence to bases 977-1,009 in the *CNGA3* CDS, with lower case 'a' representing the mutation site. The amplified product was treated with *Dpn*I to remove the methylated template plasmid, and ExNase II was used to cyclize the linear DNA. Subsequently, the resulting pcDNA3.1-CNGA3-p.S334F plasmid was transformed into *E.coli* DH5α competent cells (Takara Bio Inc.), inoculated into Luria-Bertani (LB) solid medium (Thermo Fisher Scientific Inc.) supplemented with ampicillin (Amp+) (Beyotime Biotechnology) and subjected to 12 h of inverted culture. Single clones were selected and inoculated into LB liquid medium (Amp+) at 37˚C for amplification. Plasmid DNA was then extracted from the bacteria using an EndoFree Plasmid Midi Kit (Jiangsu CoWin Biotech Co., Ltd.), and the experimental steps were as described by the manufacturer.

A pcDNA3.1-CNGA3-p.R189fs mutant plasmid was also generated. The mutation-specific primers were as follows: Forward primer (p.R189fs-F): 5'-ATTTGCAGtGGCCTGTTTCGATGAGCTGCAGT-3' (plasmid positions, 1,550-1,580) which corresponds to bases 559-589 in the *CNGA3* CDS, with lower case 't' indicating the mutation site between 566 and 567; and reverse primer (p.R189fs-R): 5'-AACAGGCCaCTGCAAATAAGCAGATACCAGTTATAGA-3' (plasmid

positions, 1,530-1,565), which corresponds to the reverse complementary sequence to bases 539-574, with lower case 'a' indicating the mutation site. The plasmid construction process was analogous to that described for pcDNA3.1-CNGA3-p.S334F. All constructed plasmids were verified by sequencing.

Cell culture and transfection. 293T cells (Guangzhou Ubigene Biosciences Co., Ltd.) were cultured at 37˚C in a 5% CO_2 atmosphere in Dulbecco's modified Eagle's medium (Thermo Fisher Scientific Inc.), supplemented with 10% fetal bovine serum (Thermo Fisher Scientific Inc.) and 1% penicillin-streptomycin. When cell confluence reached 70-80%, the plasmids were mixed with polyethyleneimine (PEI) to form a DNA-PEI complex. DNA (2 μg) was added to the cells and incubated at 37˚C for 48 h prior to the execution of subsequent experiments.

Western blotting. After rinsing with PBS, total protein was extracted from the cells by treatment with RIPA buffer (Beijing Solarbio Science & Technology Co., Ltd.; cat. no. R0020) and PMSF (cat. no. P0100). The total protein concentration was then determined using the BCA method with BSA as the standard. A total of 20 μg total protein/lane was separated using SDS-PAGE (separation gel 10%, concentrating gel 5%) and transferred onto a polyvinylidene fluoride (PVDF) membrane. The membrane was blocked with 5% skimmed milk powder for 1 h at 37˚C to prevent nonspecific binding. FLAG-tagged CNGA3 protein was then detected using a FLAG antibody (product no. F3165-1MG; 1:5,000; Sigma-Aldrich; Merck KGaA) and incubated at 4˚C for 14 h. GAPDH served as a loading control and was detected using a GAPDH antibody (cat. no. 2118S; 1:5,000; Cell Signaling Technology) and incubated at 4˚C for 14 h. The blot was then incubated with a horseradish peroxidase-conjugated secondary antibody (cat. no. SE134; 1:5,000; Beijing Solarbio Science & Technology Co., Ltd.) at room temperature for 1 h. Subsequently, a luminescent solution was applied to the PVDF membrane. NcmECL Ultra Luminol/Enhancer Reagent (A) was mixed with NcmECL Ultra Stabilized Peroxide Reagent (B) in equal proportions to make a luminescent solution (New Cell & Molecular Biotech Co., Ltd.). Images were captured using NiceAlliance Q9 software (Uvitec Ltd.). Experiments were repeated three times.

Bioinformatics analysis of CNGA3 protein expression. Protein distribution data were retrieved from the Human Protein Atlas (HPA; https://www.proteinatlas.org/). CNGA3 RNA levels in the brain were retrieved from the HPA Brain Resource (https://www.proteinatlas.org/ENSG00000144191-CNGA3/brain), which integrates and normalizes RNAseq data from the Genotype-Tissue Expression (GTEx) project for the brain and retina; the GTEx project collects and analyzes human postmortem tissues, with RNA-sequencing performed on 36 tissue types using RSEMv1.3.0 (v8) (https://deweylab.github.io/RSEM/). The GTEx retina data are based on EyeGEx data reported by Ratnapriya *et al* (14), with transcript abundance estimated using Kallisto v0.48.0 (https://pachterlab.github.io/kallisto/) with Ensembl version 109 as the reference genome. The RNA tissue expression results for CNGA3 were obtained by searching the consensus dataset in the HPA Tissue Resource for 'CNGA3' (https://www.proteinatlas.org/ENSG00000144191-CNGA3/tissue). The consensus dataset in the HPA integrates transcriptomics data from HPA and GTEx datasets for 55 tissue types through an internal normalization pipeline. CNGA3 single-cell expression results were obtained by searching the Single Cell Type and Single Cell Resource sections of the HPA for 'CNGA3' (https://www.proteinatlas.org/ENSG00000144191-CNGA3/single+cell). This analysis integrates single-cell information for 31 human tissues from various databases, including the Single Cell Expression Atlas, Human Cell Atlas, Gene Expression Omnibus, Tabula Sapiens, Allen Brain Atlas and European Genome-phenome Archive. Transcript per million (TPM) values were rescaled to a sum of one million TPM following the removal of non-coding transcripts. Within each data source, the TPM values of all samples were normalized separately using the trimmed mean of the M values to allow between-sample comparisons. The final normalized transcript expression values, denoted as normalized parts per million (nTPM) markers, were calculated for each gene in each sample, with nTPM values <0.1 excluded from visualization in the HPA. Prediction of protein stability after *CNGA3* mutation was performed using the DEZYME tool (https://soft.dezyme.com/query/create/pop), with $\Delta\Delta G$ <0 meaning a stabilizing mutation.

Statistical analysis. Protein expression results in the *in vitro* experiment are presented as the mean ± SD. The difference between wild-type and CNGA3:p.S334F groups was analyzed using an unpaired Student's t-test. $P<0.05$ was considered to indicate a statistically significant difference. In order to assess whether the distribution of *CNGA3* mutation sites in the structural and non-structural domains was statistically significant, the distributional characteristics of the mutation sites were systematically analyzed in this study using a one-sample hypothesis test. The null hypothesis (H0) of the test posited that there was no statistically significant difference in the distribution of mutation sites between the structural and non-structural domains. By contrast, the alternative hypothesis (H1) predicted that the proportion of mutation sites in the structural domains would be significantly higher than that in the non-structural domains. The significance level of the test was set at $\alpha=0.05$. The statistical analysis was conducted using GraphPad Prism (version 10.4) and R software (version 4.1.2).

Results

Clinical data of the patient. The patient was a 9-year-old girl with COD whose parents exhibited no signs of any associated eye disease. The child was first diagnosed with COD in September 2020. She had a visual acuity of 20/100 in both eyes and mild nystagmus. Fundus photography revealed a loss of foveal reflex in both eyes (Fig. 1A and B). OCT revealed low ganglion cell thickness and a retinal nerve fiber layer thinner than normal (Fig. 1C-F) (15). ERG demonstrated decreased dark-adapted b-wave and a-wave amplitudes and approximately normal oscillatory potential amplitudes in both eyes (Fig. 2). The patient was prescribed glasses for full correction of hyperopia and astigmatism. However, her visual acuity improved by no more than one line during follow-up. Upon re-examination on December 5, 2024, her visual acuity was unchanged at 20/100 in each eye. Her electroretinogram exhibited a slight improvement, although it remained markedly abnormal (Fig. S2).

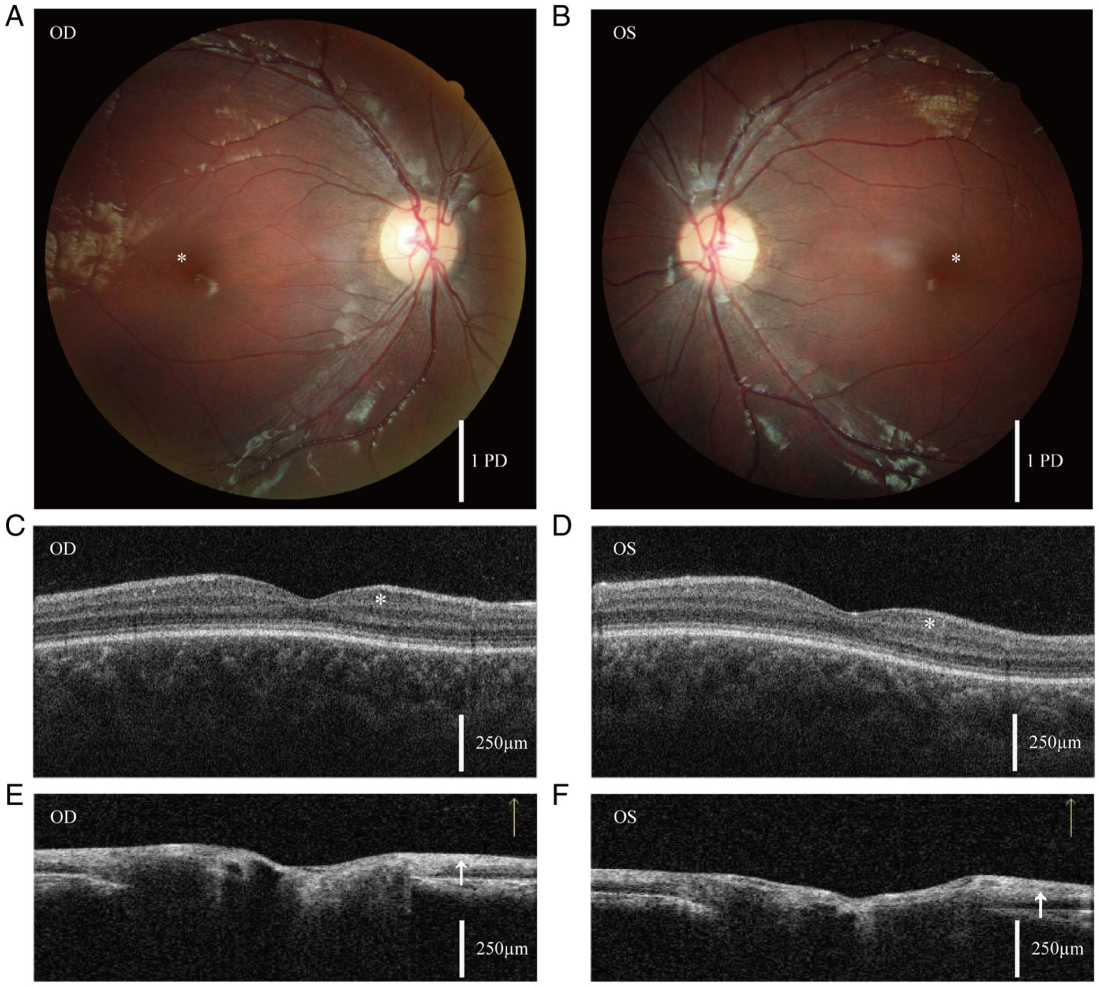

Figure 1. Fundus photography and OCT. (A and B) Fundus photographs of the right and left eyes of the patient, respectively. The asterisk indicates disappearance of the foveal reflex. Scale bar, 1 optic disc PD. Since PD varies among individuals, it serves as a standard for distance and range in fundus examinations. (C and D) Measurements of the GCC in the macula of the right and left eyes, respectively. The asterisk indicates that OCT examination revealed a thinner than normal ganglion cell layer, with an average GCC thickness of 84 μm in the right eye and 85 μm in the left eye. (E and F) Measurements of the optic nerve head in the right and left eyes, respectively, reveal that the retinal nerve fiber layer, indicated by the arrows, is also thinner than normal. The average retinal nerve fiber layer thickness is 99 μm in the right eye and 95 μm in the left eye. Scale bar in the OCT images, 250 μm. OCT, optical coherence tomography; OD, *oculus dexter*/right eye; OS, *oculus sinister*/left eye; PD, papilla diameter; GCC, ganglion cell complex.

CNGA3 mutations contributing to COD. Whole-exome sequencing of the proband and her parents (Fig. 3A) was performed (16). Genetic analysis revealed compound heterozygous *CNGA3* mutations in the proband, including a known missense single-nucleotide variant (*CNGA3*:c.C1001T) and a previously unreported frameshift mutation (*CNGA3*:c.566_567insT) (Table I). The mother was a carrier of the c.C1001T mutation, which results in substitution of serine with phenylalanine at codon 334 (p.S334F). The novel c.566_567insT frameshift mutation was inherited from her father, who was a carrier. Fig. S3 presents the nucleic acid sequence following the *CNGA3*:c.566_567insT:p.R189fs mutation, highlighting the insertion of base T between positions 566 and 567 in the cDNA sequence. This mutation leads to a TGA premature stop codon at position 194, thereby reducing the number of amino acids in the reading frame from 694 to 193, resulting in a shorter, less stable protein. These mutations were validated using Sanger sequencing, which confirmed the *CNGA3*:c.C1001T:p.S334F mutation in the patient and her mother (Fig. 3B) and the *CNGA3*:c.566_567insT:p.R189fs mutation in the patient and her father (Fig. 3C). Clonal sequencing of *CNGA3*:c.566_567insT:p.R189fs yielded results consistent with this mutation (Fig. 3D). Bioinformatics analysis reveals that CNGA3 is highly expressed in the brain (Fig. S4A), retina (UniProtKB, Q16281; Fig. S4B), neuronal protrusions, axons and cone photoreceptor cells (Fig. S4C).

Effect of CNGA3 mutations on protein structure and function. The p.S334F and p.R189fs mutations are located on the ion-transport (ion-trans) structural domain of CNGA3 protein. Notably, p.R189fs results in a truncated protein product that only retains the ion-trans domain and lacks the cysteine-rich CAP domain-extended domain (CAP-ED) and cyclic nucleotide-gated ligand-binding zinc finger-like (CLZ) domain (Fig. 3E). The conservativeness of the two mutant loci, p. R189fs and p.S334F, was evaluated, and the mutations were found to be located in regions that are highly conserved across species (Fig. 3F). Mutations in highly conserved protein regions may impact their functionality (17). The p.S334F mutation affects a conserved residue in the ion-trans domain and is

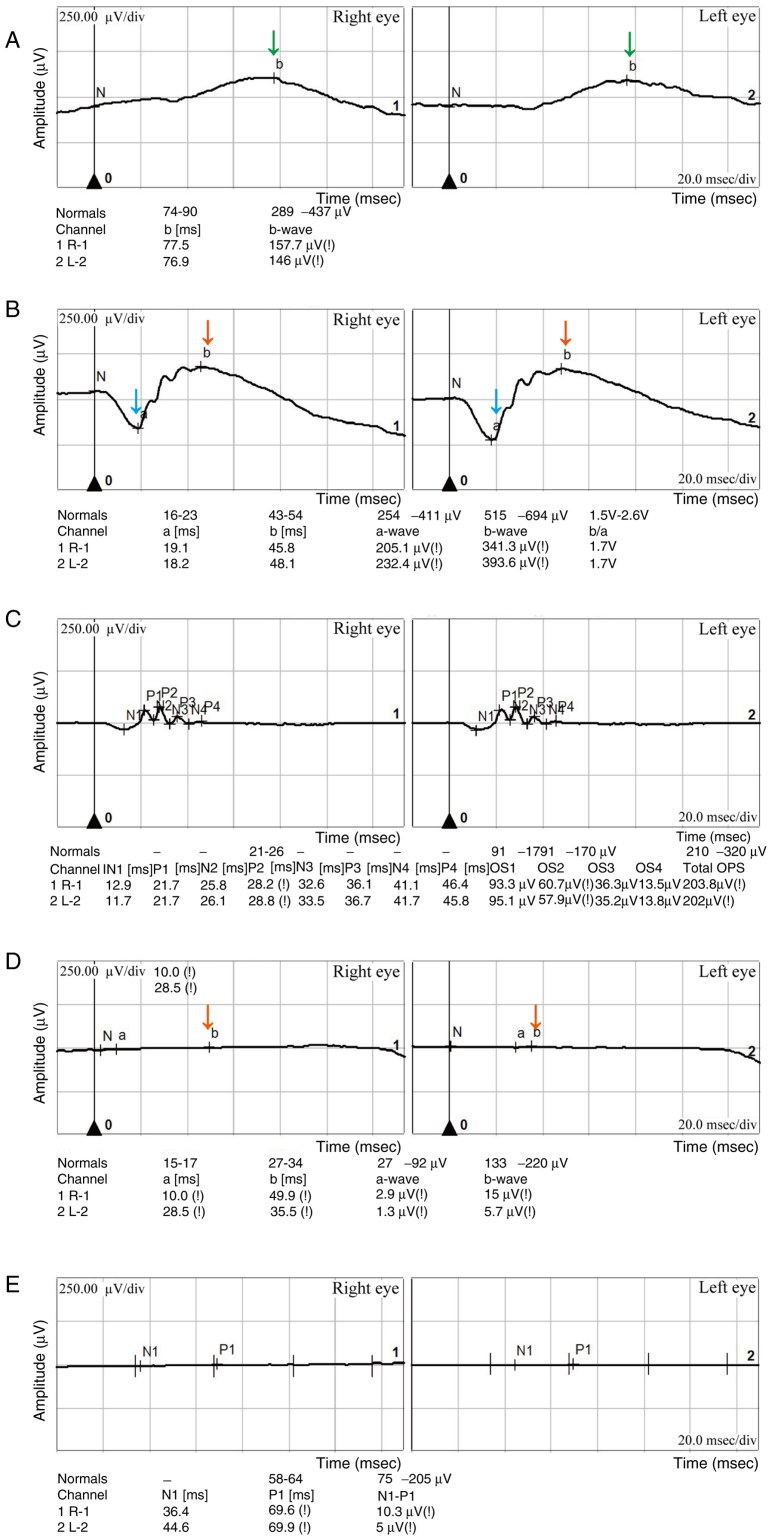

Figure 2. Retinal electroretinogram results. (A) Dark-adapted 0.01 ERG showing b-wave amplitudes of 157.7 and 146 μV in the right and left eye, respectively. The dark-adapted b-wave amplitudes (indicated by the green arrows) are diminished in both eyes compared with the normal range (289-437 μV). This dysfunction may involve rod photoreceptors or be selective to post-phototransduction processes or rod bipolar cells within the retina. (B) Dark-adapted 3.0 ERG showing a-wave amplitudes of 205.1 and 232.4 μV in the right and left eye, respectively. This indicates a reduction in the a-wave amplitude (indicated by the blue arrows), with both eyes measuring below the normal range (254-411 μV). The b-wave amplitudes (indicated by the red arrows) are 341.3 and 393.6 μV in the right and left eye, respectively, both below the normal range (515-694 μV). The dark-adapted 3.0 ERG reflects both the rod and cone cell activity, with the rod cell system being the predominant contributor in the normal retina. Therefore, these findings indicate that the cellular photoreceptors in the patient are dysfunctional. (C) Oscillatory potential ERG indicates an approximately normal oscillatory potentials response, reflecting the absence of long-synapse cell signaling, consistent with normal expectations. (D) Light-adapted 3.0 ERG demonstrates a pronounced reduction in b-wave amplitude (indicated by the red arrow). The amplitudes of the right and left eye are 15 and 5.7 μV, respectively, markedly below the normal range (133-220 μV). These results suggest the possibility of cone cell photoreceptor dysfunction. (E) Analysis by 30-Hz flicker ERG demonstrates an N1-P1 wave amplitude of 10.3 and 5 μV in the right and left eye, respectively, below the typical range (75-205 μV) in both eyes. This indicates the potential presence of anomalies in cone cells and their posterior retinal structures. The clinical manifestations of decreased visual acuity, night blindness and impaired color vision in the patient may be attributed to dysfunction of the cone and rod photoreceptors and their associated retinal structures in both eyes. ERG, electroretinography.

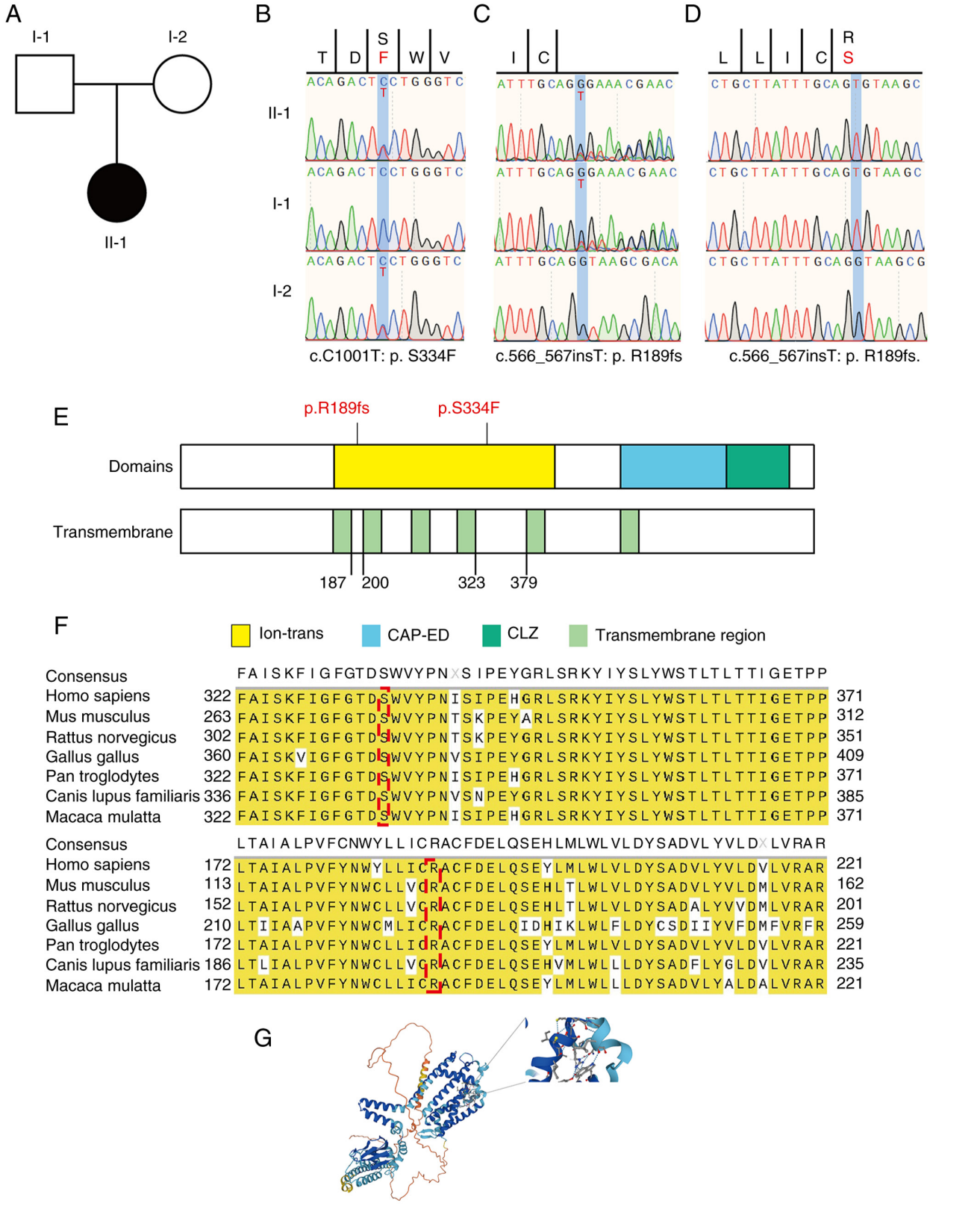

Figure 3. *CNGA3* mutations associated with retinal cell dystrophy. (A) Family relationship diagram of the patient, a 9-year-old girl with evidence of retinal dystrophy. Neither the father (I-1) or mother (I-2e) of the child is afflicted with the disease, and the girl (II-1) was the first to manifest this condition. The pattern of inheritance may be autosomal recessive. (B) The *CNGA3*:c.C1001T:p.S334F mutation was identified in the precursor and her mother and (C) the *CNGA3*:c.566_567insT:p.R189fs mutation was detected in the patient and her father by the whole-exome sequencing and data analysis of peripheral blood. (D) Clonal sequencing of *CNGA3*:c.566_567insT:p.R189fs yielded results consistent with those in (C). These data indicate that the patient inherited distinct compound heterozygous mutations from both parents. (E) Schematic of the CNGA3 structural domains, namely ion-trans, CAP-ED and CLZ. The p.S334F and p.R189fs mutations both occur in the ion-trans structural domain, indicating that they may affect the transmembrane transport of ions. (F) Conservativeness analysis of the two mutant loci, p.R189fs and p.S334F, reveals that the mutations are located in regions that are highly conserved across species. This suggests that they are likely to impact protein function. (G) Schematic showing the location of the *CNGA3*:p.S334F mutant amino acids in the molecular structure. CNGA3, cyclic nucleotide-gated channel subunit α 3; ion-trans, ion transport; CAP-ED, cysteine-rich CAP domain-extended domain; CLZ, cyclic nucleotide-gated ligand-binding zinc finger-like.

Table I. Detailed information of the variants *CNGA3*(p. R189fs) and *CNGA3*(p.S334F).

Carriers	Chr	Pos (GRCh37)	Ref.	Alt	AD	ChinaMap	ESP	GnomAD	1000G	SIFT	Polyphen-2	CADD
I-1 and II-1	2	99006237	G	GT	I-1: 8,8 and II-1: 7,11	-	-	-	-	-	-	5.571691
I-2 and II-1	2	99012634	C	T	I-2: 32,24 and II-1 :38,50	-	-	-	-	0.003, D	0.173, B	-

Carriers are the family members who carry the mutations. CNGA3, cyclic nucleotide-gated channel subunit a 3; Chr, chromosome; Pos (GRCh37), position on chromosome according to Genome Reference Consortium Human Build 37; Ref., reference base; Alt, alternate base; AD, allele depth; ESP, Exome Sequencing Project; GnomAD, Genome Aggregation Database; 1000G, 1000 Genomes; SIFT, Sorting Intolerant from Tolerant; Polyphen-2, Polymorphism Phenotyping v2; CADD, Combined Annotation Dependent Depletion.

predicted to be harmful based on SIFT and PolyPhen analyses (SIFT 0.003, damaging; Polyphen2_HVAR 0.863, possibly damaging; PolyPhen2_HDIV 0.965, probably damaging). The protein structure and stability were then predicted to gain insights into the impact of the mutation on the protein. The p.S334F mutation was predicted to decrease protein stability, with a $\Delta\Delta G$ value of 0.74 kcal/mol. A schematic showing the location of the *CNGA3* mutation in the molecular structure is presented in Fig. 3G. Of the total 151 *CNGA3* mutations reported in humans, 40 are associated with COD (Table II). Further hypothesis testing of the relationship between the mutations and structural domains of CNGA3 proteins yielded $P<0.0011$ ($\alpha=0.05$), indicating the enrichment of mutations in structural domains (Fig. 4).

In vitro analysis of CNGA3 mutations. To further investigate the effects of these mutations on protein expression, wild-type and mutant CNGA3 proteins were expressed in 293T cells and analyzed by western blotting (Fig. S5). The FLAG-tagged wild-type CNGA3 protein appeared as two distinct bands, specifically, a main band at 81.7 kDa and an additional band of higher molecular weight (~100 kDa), likely representing a post-translationally modified protein. The S334F mutation resulted in significantly increased CNGA3 protein expression compared with that of wild-type *CNGA3*, but notably lacked the ~100 kDa band (Fig. 5). Given that S334 is a potential phosphorylation site, we hypothesize that the S334F mutation might prevent phosphorylation at this position. By contrast, the c.566_567insT:p.R189fs mutation produced a truncated protein with a molecular weight of 16.0 kDa, consistent with the predicted premature termination of protein synthesis.

Discussion

The present study reports a case of COD with novel compound heterozygous *CNGA3* mutations. Although the *CNGA3*:p.S334F mutation was predicted to reduce CNGA3 protein stability, western blotting results revealed that CNGA3 protein expression was abnormally increased following this mutation. It is hypothesized that this may be attributed to the mutation preventing protein phosphorylation. In addition, no additional protein band was evident above the CNGA3:p.S334F protein, whereas a band was clearly visible above the wild-type protein. Serine is a common phosphorylation site (18,19). In a study of spastin phosphorylation, Zhang *et al* (20) compared wild-type spastin with a mutant in which 2 potential phosphorylation sites were mutated to alanine. They found that the quantity of the wild-type protein was markedly diminished compared with that of the protein with mutated phosphorylation sites, indicating that protein degradation may occur as a result of protein phosphorylation. Kaushik and Cuervo (21) found that the treatment of cells with oleate-conjugated albumin increased total perilipin 2 (PLIN2) content 1.5-fold, with a more pronounced (5-fold) increase in the phosphorylated form. The phosphorylation of PLIN2 was undetectable when chaperone-mediated autophagy was blocked by lysosome-associated membrane protein 2A knockdown, while the amount of PLIN2 protein was concurrently increased. This suggests that phosphorylation may have played a role in promoting PLIN2 degradation

Table II. *CNGA3* mutations associated with COD and associated clinical information.

Mutation					Best visual acuity		Fundus		Electroretinogram		
DNA	Amino acid	State	Sex	Age at examination, years	Right	Left	Right	Left	Rods	Cones	First author, year (Refs.)
c.62C>G	p.S21*	Heterozygous	M	2.0	-	-	PFR	PFR	Moderately reduced	Extinguished	Li *et al*, 2014 (32)
c.67C>T	p.R23*	Heterozygous	F	0.4	PO	PO	TDP, PM	TDP, PM	Mildly reduced	Extinguished	Li *et al*, 2014[a] (32); Johnson *et al*, 2004 (67); Ellingford *et al*, 2016 (68)
c.284C>T	p.P95L	Heterozygous	-	-	-	-	-	-	-	-	Thiadens *et al*, 2010 (31)
c.396-11C>G	-	Heterozygous	F	4.0	-	-	Normal	Normal	Moderately reduced	Severely reduced	Li *et al*, 2014 (32)
		Homozygous	M	0.6	0.20	0.20	ARA, TDP	ARA, TDP	Moderately reduced	Severely reduced	Li *et al*, 2014 (32)
		Heterozygous	M	5.0	0.40	0.40	TDP, PM	TDP, PM	Moderately reduced	Extinguished	Li *et al*, 2014 (32)
c.512G>A	p.W171*	Homozygous	F	1.2	-	-	Normal	Normal	Mildly reduced	Mildly reduced	Li *et al*, 2014 (32)
c.513G>T	p.W171C	Heterozygous	F	1.5	-	-	PM	PM	Mildly reduced	Extinguished	Li *et al*, 2014 (32)
c.566_567insT	p.R189fs	Heterozygous	F	9.0	0.20	0.20	PM	PM	Moderately reduced	Severely reduced	Present study
c.661C>T	p.R221*	Heterozygous	F	2.0	-	-	-	-	Moderately reduced	Severely reduced	Li *et al*, 2014[a] (32); Johnson *et al*, 2004 (67)
		Heterozygous	M	4.0	PO	PO	ARA	ARA	Moderately reduced	Severely reduced	
c.667C>T	p.R223W	Homozygous	F	2.0	-	-	-	-	Mildly reduced	Severely reduced	Li *et al*, 2014 (32); Wissinger *et al*, 2001 (28)
c.671C>T	p.T224I	Heterozygous	M	3.0	-	-	TDP	TDP	Moderately reduced	Severely reduced	Li *et al*, 2014 (32)
		Heterozygous	M	2.3	-	-	NFR	NFR	Moderately reduced	Moderately reduced	Li *et al*, 2014 (32)
c.674-2A>C	-	Heterozygous	M	2.3	-	-	NFR	NFR	Moderately reduced	Moderately reduced	Li *et al*, 2014 (32)
c.682G>A	p.E228K	Heterozygous	M	47.0	-	-	-	MA	-	-	Thiadens *et al*, 2010[a](31); Reuter *et al*, 2008 (69)
c.773C>G	p.P258R	Heterozygous	F	4.0	-	-	Normal	Normal	Moderately reduced	Extinguished	Li *et al*, 2014 (32)
c.778G>A	p.D260N	Heterozygous	M	2.0	-	-	PFR	PFR	Moderately reduced	Extinguished	Li *et al*, 2014[a] (32); Wissinger *et al*, 2001 (28)
c.829C>T	p.R277C	Heterozygous	F	15.0	0.50	0.50	-	-	-	-	Wissinger *et al*, 2001 (28)
		Heterozygous	F	2.0	-	-	-	-	Moderately reduced	Severely reduced	Li *et al*, 2014 (32)
c.830G>A	p.R277H	Heterozygous	M	1.5	-	-	TDP, ARA	TDP, ARA	Mildly reduced	Extinguished	Li *et al*, 2014[a] (32); Wissinger *et al*, 2001 (28)
c.847C>T	p.R283W	Heterozygous	F	15.0	0.50	0.50	-	-	-	-	Wissinger *et al*, 2001[a](28); Kohl *et al*, 1998 (37)
		Heterozygous	M	3.0	-	-	TDP	TDP	Moderately reduced	Severely reduced	Li *et al*, 2014[a] (32); Kohl *et al*, 1998 (37)
		Heterozygous	F	1.5	-	-	PM	PM	Mildly reduced	Extinguished	

Table II. Continued.

Mutation		State	Sex	Age at examination, years	Best visual acuity		Fundus		Electroretinogram		First author, year (Refs.)
DNA	Amino acid				Right	Left	Right	Left	Rods	Cones	
c.872_873del	p.T291Rfs*77	Heterozygous	F	8.0	-	-	MA	MA	-	-	Li *et al*, 2014 (32)
		Heterozygous	F	4.5	0.10	0.20	TDP	TDP	Mildly reduced	Severely reduced	Li *et al*, 2014 (32)
c.955T>C	p.C319R	Homozygous	F	10.0	CF (1 M)	CF (1 M)	MA	MA	Moderately reduced	Severely reduced	Shaikh *et al*, 2015 (5)
c.967G>C	p.A323P	Heterozygous	F	-	-	-	-	-	-	-	Carss *et al*, 2017 (70)
c.989T>C	p.F330S	Heterozygous	M	0.3	PL	PL	-	-	Mildly reduced	Severely reduced	Li *et al*, 2014 (32)
		Heterozygous	F	6.0	0.08	0.08	NFR, TDP	TDP	Mildly reduced	Severely reduced	Li *et al*, 2014 (32)
c.1001C>T	p.S334F	Heterozygous	M	2.5	0.40	0.40	ARA	ARA	Moderately reduced	Extinguished	Li *et al*, 2014 (32)
c.1074G>A	p.W358*	Heterozygous	M	28.0	0.10	0.10	ARA, MA	ARA, MA	Moderately reduced	Extinguished	Li *et al*, 2014 (32)
		Heterozygous	M	0.5	PL	PL	ARA, NFR	ARA, NFR	Mildly reduced	Severely reduced	Li *et al*, 2014 (32)
		Heterozygous	F	4.0	-	-	Normal	Normal	Moderately reduced	Severely reduced	Li *et al*, 2014 (32)
c.1116dup	p.V373Rfs*4	Heterozygous	F	4.0	-	-	Normal	Normal	Moderately reduced	Extinguished	Li *et al*, 2014 (32)
c.1306C>T	p.R436W	Heterozygous	F	1.0	PO	PO	Normal	Normal	Mildly reduced	Extinguished	Li *et al*, 2014[a] (32); Wissinger *et al*, 2001 (28)
		Homozygous	F	2.0	PO	PO	PM	PM	Moderately reduced	Extinguished	
c. 1315C>T	p.R439W	Heterozygous	M	0.3	PL	PL	-	-	Mildly reduced	Severely reduced	Li *et al*, 2014[a] (32); Reuter *et al*, 2008 (69)
		Heterozygous	M	2.5	0.40	0.40	ARA	ARA	Moderately reduced	Extinguished	
c.1495C>T	p.R499*	Heterozygous	F	1.0	PO	PO	Normal	Normal	Mildly reduced	Extinguished	Li *et al*, 2014 (32)
		Heterozygous	M	5.0	0.40	0.40	TDP, PM	TDP, PM	Moderately reduced	Extinguished	Li *et al*, 2014 (32)
c.1513C>G	p.P505A	Heterozygous	-	-	-	-	-	-	-	-	Huang *et al*, 2016 (29)
c.1537G>C	p.G513R	Heterozygous	-	-	-	-	-	-	-	-	Huang *et al*, 2016 (29)
c.1556T>C	p.M519T	Heterozygous	-	-	-	-	-	-	-	-	Huang *et al*, 2016 (29)
c.1585G>A	p.V529M	Homozygous	F	1.1	-	-	Normal	Normal	Moderately reduced	Severely reduced	Li *et al*, 2014[a] (32); Kohl *et al*, 1998 (37)
		Homozygous	M	5.0	-	-	Normal	Normal	Mildly reduced	Severely reduced	
		Homozygous	F	0.6	PO	PO	-	-	Mildly reduced	Severely reduced	
		Heterozygous	M	28.0	0.10	0.10	ARA, MA	ARA, MA	Moderately reduced	Extinguished	
		Heterozygous	M	4.0	PO	PO	ARA	ARA	Moderately reduced	Severely reduced	
		Heterozygous	F	6.0	0.08	0.08	NFR, TDP	TDP	Mildly reduced	Severely reduced	
		Heterozygous	M	17.0	0.10	0.10	PM	PM	Mildly reduced	Moderately reduced	
		Heterozygous	M	1.5	-	-	TDP, ARA	TDP, ARA	Mildly reduced	Extinguished	
		Heterozygous	F	4.5	0.10	0.20	TDP	TDP	Mildly reduced	Severely reduced	

Table II. Continued.

Mutation		State	Sex	Age at examination, years	Best visual acuity		Fundus		Electroretinogram		First author, year (Refs.)
DNA	Amino acid				Right	Left	Right	Left	Rods	Cones	
c.1597G>C	p.D533H	Homozygous	F	3.0	-	-	ARA	ARA	Mildly reduced	Extinguished	Li *et al*, 2014 (32)
c.1618G>A	p.V540I	Heterozygous	-	-	-	-	-	-	-	-	Thiadens *et al*, 2010 (31)
c.1641C>A	p.F547L	Heterozygous	F	32.0	<0.50	<0.50	-	-	-	-	Wissinger *et al*, 2001 (28); Kohl *et al*, 1998 (37)
c.1688G>A	p.R563H	Heterozygous	F	32.0	<0.50	<0.50	-	-	-	-	Wissinger *et al*, 2001 (28); Ellingford *et al*, 2016 (68)
c.1709G>A	p.S570N	Heterozygous	M	17.0	0.10	0.10	PM	PM	Mildly reduced	Moderately reduced	Li *et al*, 2014 (32)
c.1768G>A	p.E590K	Heterozygous	M	2.0	-	-	PFR	PFR	Moderately reduced	Extinguished	Li *et al*, 2014 (32); Nishiguchi *et al*, 2005 (38)
c.1856C>T	p.A619V	Heterozygous	-	-	-	-	-	-	-	-	Thiadens *et al*, 2010 (31)
c.1877T>G	p.L626R	Heterozygous	-	-	-	-	-	-	-	-	Huang *et al*, 2016 (29)
c.1975A>T	p.K659*	Heterozygous	F	8.0	-	-	MA	MA	-	-	Li *et al*, 2014 (32)

[a]Clinical data in the specified row originates from the indicated reference. * in the amino acid column indicates a stopgain or nonsense mutation. ARA, attenuated retinal arterioles; CF (1 M), counting fingers at a distance of 1 m; F, female; M, male; MA, macular atrophy; NFR, no foveal reflex; PFR, poor foveal reflex; PL, pursuing light; PM, pigmentation in macular; PO, pursuing object; TDP, temporal disc pall.

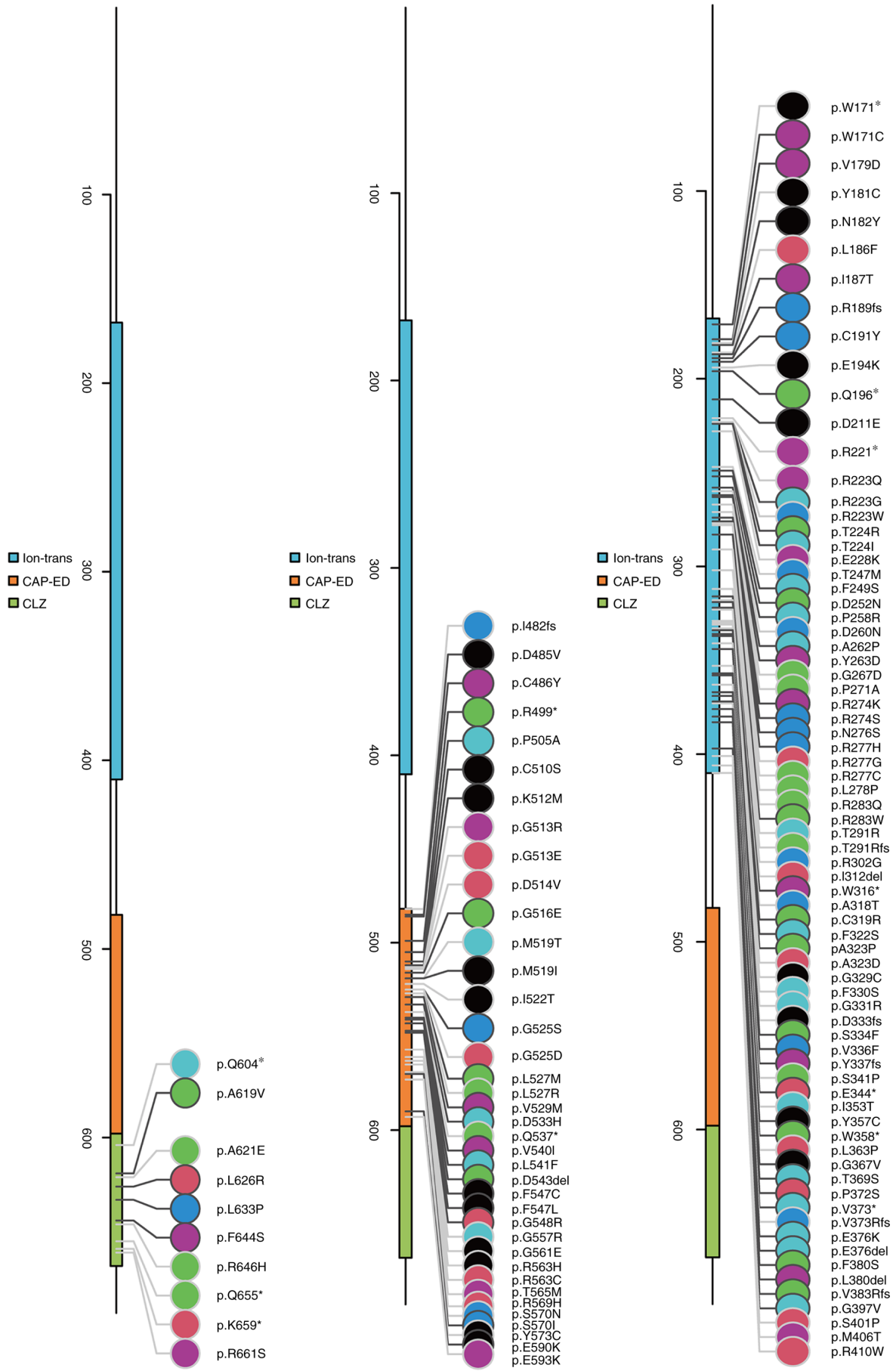

Figure 4. Position of known mutations in *CNGA3*. *CNGA3* mutations in the ion-trans, CAP-ED and CLZ structural domains. CNGA3, cyclic nucleotide-gated channel subunit α 3; ion-trans, ion transport; CAP-ED, cysteine-rich CAP domain-extended domain; CLZ, cyclic nucleotide-gated ligand-binding zinc finger-like.

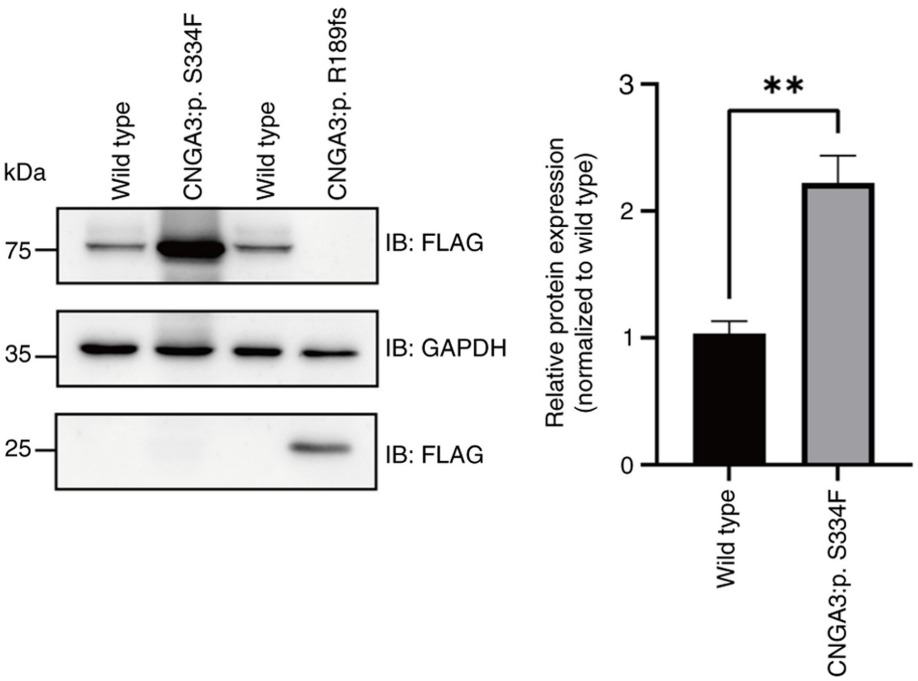

Figure 5. Western blotting of CNGA3 wild-type and mutant proteins in cells transfected with pcDNA3.1-CNGA3, pcDNA3.1-CNGA3-p.S334F and pcDNA3.1-CNGA3-p.R189fs plasmids. This reveals that the molecular weight of the *CNGA3*:c.C1001T:p.S334F mutant was identical to that of wild-type CNGA3, and its expression was significantly elevated. By contrast, the molecular weight of the *CNGA3*:c.566_567insT:p.R189fs mutant was markedly reduced compared with that of wild-type CNGA3 due to the presence of a premature stop codon. **P<0.01. CNGA3, cyclic nucleotide-gated channel subunit α 3.

or preventing its accumulation. These findings for other proteins support the hypothesis that the *CNGA3*:p.S334F mutation prevents protein phosphorylation, which would otherwise lead to protein degradation. Although the inherent structural instability of the mutation may also contribute to protein degradation, this effect appears to have been less pronounced than the impact of phosphorylation changes on the protein. Consequently, the expression of the CNGA3 protein following mutation was significantly higher than that of the wild-type protein, likely due to a lack of degradation. However, it must be acknowledged that the lack of detection of protein phosphorylation levels in the western blot experiments is a limitation of the present study. The novel *CNGA3*:p.R189fs mutation creates a premature stop codon that leads to the deletion of the key CAP-ED and CLZ structural domains, which is predicted to disrupt the normal tetrameric structure of the CNGA3 protein. This structural disruption would be expected to impair the normal function of the ion channel in the retina, leading to symptoms such as decreased visual acuity and other visual disturbances. To the best of our knowledge, the present study is the first to identify the *CNGA3*:p.R189fs mutation in COD, and the only *in vitro* study of *CNGA3* mutations in COD.

The main features of COD include decreased visual acuity, impaired color recognition, and increased sensitivity to light, typically manifested during the first or second decade of life (22). Mutations in genes such as *CNGA3*, calcium voltage-gated channel subunit α2δ4, *CNGB3*, phosphodiesterase 6C (*PDE6C*), *PDE6H* and ATP-binding cassette subfamily A member 4 have been implicated in the pathogenesis of COD (23-27). The association between *CNGA3* and COD was first reported by Wissinger *et al* (28) in a study of 258 individuals with hereditary cone photoreceptor disease in 2001. Since then, several studies have identified additional *CNGA3* mutations in patients with COD (29-31). COD caused by *CNGA3* mutations follows an autosomal recessive inheritance pattern (32,33), and mutations of CNG channels often alter their plasma membrane localization and gating properties (34,35).

CNGA3 mutations are associated with hereditary cone photoreceptor disorders, particularly color blindness (OMIM: 600053) (36). Due to the absence of functional cone photoreceptors in the retina, the disease is characterized by complete color blindness, low vision, photophobia and nystagmus (37,38). The CNG3 channel comprises CNGA3 and CNGB3, which form a heterotetrametric structure with two α and two β subunits (3). Both CNGA3 and CNGB3 are implicated in cone photoreceptor disorders (39,40), and mice with *CNGA3* and *CNGB3* knockout exhibit reduced electroretinographic responses, decreased phototransduction expression and significantly increased expression of endoplasmic reticulum stress marker proteins (41). These findings suggest that mitochondrial damage may contribute to endoplasmic reticulum stress-mediated retinal cone cell death. Impaired calcium homeostasis and the mislocalization of retinal proteins may also accelerate rod cell death, while cGMP accumulation can lead to retinal cone cell stress and damage (42,43).

cGMP activates CNGA3, which triggers the G-protein-coupled cascade and leading to the opening of cation channels and depolarization of cone photoreceptors, which is essential for normal vision (44-46). CNGA3 also plays an important role in the light-evoked electrical responses in red-, green- and blue-sensitive cones (47). The mutations in *CNGA3* identified in the present case, namely p.S334F and

p.R189fs, will disrupt the transporter function of ion channels, preventing the normal depolarization of cone photoreceptor cells and thereby impair the ability to discriminate colors. In the present study, the patient exhibited reduced visual acuity and color vision deficiency. Considering that the patient was at an early stage of OCD, fundus photography did not reveal any distinctive fundus lesions and showed only a loss of foveal reflex. However, as the disease progresses, fundus imaging may be expected to reveal the presence of macular lesions or retinal pigment epithelial lesions in a bull's-eye configuration (48). Furthermore, OCT may detect the absence of the interdigitation zone early in the disease, followed by progressive destruction of the ellipsoid zone (49-51). In addition, ERG examination of the single-flash response may reveal delayed a- and b-waves and reduced light-adapted a- and b-wave amplitudes (52).

Definitive treatments to stop COD progression or severe vision loss are unavailable, with only symptomatic management through refractive correction and tinted glasses being available (53). Notably, several complementary treatments are currently being investigated, and gene therapy could emerge as a key treatment modality for hereditary retinal diseases such as COD in the future. Gene editing with CRISPR/Cas9 is currently the primary therapeutic modality in clinical trials, aiming to introduce specific nucleotide alterations into the target genome to restore normal gene expression (54-56). In addition, gene replacement therapy has been shown to enable the sustained expression of normal genes in mice with retinal disease and promote functional improvement, with treatments approved by the US Food and Drug Administration already being available (57-59). In addition, silencing the gene associated with a dominant retinal degeneration mouse model, namely guanylate cyclase activating protein 1, has been found to significantly improve photoreceptor survival, delay disease onset and enhance visual function (60-62). Other adjuvant therapies are also being investigated. These include brain-derived neurotrophic factor, pigment epithelium-derived neurotrophic factor, basic fibroblast growth factor, ciliary neurotrophic factor and rod cone viability factor, which are being explored for their potential to slow down retinal degeneration in COD (63-66).

In conclusion, the present study identified a compound heterozygous mutation in *CNGA3*, with a c.C1001T:p.S334F variant and a novel frameshift mutation c.566_567insT:p.R189fs, in a patient with COD, and demonstrated their potential impact on protein stability. The findings not only expand the spectrum of disease-causing mutations in *CNGA3* but also provide crucial insights into its role in COD pathogenesis. Integrating a literature analysis allowed the results to further reveal that specific CNGA3 structural domains may represent mutation hotspots in COD. These findings highlight potential targets for developing therapies for CNGA3-related retinal diseases.

Acknowledgements

The authors thank Dr Feng Dong of the Department of Cell Biology, School of Basic Medical Sciences, Tianjin Medical University (Tianjin, China) for technical support with plasmid construction.

Funding

This study was supported by the Project of Tianjin 131 Innovative Talent Team (grant no. 201936), Science and Technology Fund for Health of Tianjin (grant no. TJWJ2023ZD008), Science Fund for Distinguished Young Scholars of Tianjin (grant no. 17JCJQJC46000), Science and Technology Planning Project of Tianjin (grant no. 21JCYBJC00780), Jinmen Medical Talent Project of Tianjin, and Tianjin Key Medical Discipline (Specialty) Construction Project (grant no. TJYXZDXK-016A).

Availability of data and materials

The *CNGA3*:p. S334F mutation identified in the present study may be found in dbSNP (https://www.ncbi.nlm.nih.gov/snp/) under accession number rs1692907593. The datasets analyzed in the current study are not publicly available because the family did not consent to the release of their full sequencing information due to privacy concerns; however, they may be requested from corresponding author XS.

Authors' contributions

RS and YW performed data screening, data analysis and statistical analysis, and wrote the manuscript. SC performed Sanger sequencing. WZ and MP participated in data analysis. RS and YW constructed plasmids. RS, YL, and DJ performed cell transfection, protein extraction and western blotting experiments. JL and XS conceived and designed the study, reviewed the manuscript, and confirm the authenticity of all the raw data. All authors read and approved the final version of the manuscript.

Ethics approval and consent to participate

The present study was approved by the Ethics Committee of Tianjin Eye Hospital (Tianjin, China; approval no. 202015) and was performed in accordance with Declaration of Helsinki guidelines. Written informed consent for participation in the study was obtained from the participants and the legal guardian of the child.

Patient consent for publication

The participants and the legal guardian of the child provided written consent for publication.

Competing interests

The authors declare that they have no competing interests.

References

1. Tsang SH and Sharma T: Progressive cone dystrophy and cone-rod dystrophy (XL, AD, and AR). Adv Exp Med Biol 1085: 53-60, 2018.
2. Gill JS, Georgiou M, Kalitzeos A, Moore AT and Michaelides M: Progressive cone and cone-rod dystrophies: Clinical features, molecular genetics and prospects for therapy. Br J Ophthalmol 103: 711-720, 2019 (Epub ahead of print).

3. Zheng X, Hu Z, Li H and Yang J: Structure of the human cone photoreceptor cyclic nucleotide-gated channel. Nat Struct Mol Biol 29: 40-46, 2022.
4. Sun W and Zhang Q: Diseases associated with mutations in CNGA3: Genotype-phenotype correlation and diagnostic guideline. Prog Mol Biol Transl Sci 161: 1-27, 2019.
5. Shaikh RS, Reuter P, Sisk RA, Kausar T, Shahzad M, Maqsood MI, Yousif A, Ali M, Riazuddin S, Wissinger B and Ahmed ZM: Homozygous missense variant in the human CNGA3 channel causes cone-rod dystrophy. Eur J Hum Genet 23: 473-480, 2015.
6. Li H, Handsaker B, Wysoker A, Fennell T, Ruan J, Homer N, Marth G, Abecasis G and Durbin R; 1000 Genome Project Data Processing Subgroup:The sequence alignment/map format and SAMtools. Bioinformatics 25: 2078-2079, 2009.
7. Wang K, Li M and Hakonarson H: ANNOVAR: Functional annotation of genetic variants from high-throughput sequencing data. Nucleic Acids Res 38: e164, 2010.
8. 1000 Genomes Project Consortium; Auton A, Brooks LD, Durbin RM, Garrison EP, Kang HM, Korbel JO, Marchini JL, McCarthy S, McVean GA and Abecasis GR: A global reference for human genetic variation. Nature 526: 68-74, 2015.
9. Karczewski KJ, Francioli LC, Tiao G, Cummings BB, Alföldi J, Wang Q, Collins RL, Laricchia KM, Ganna A, Birnbaum DP, *et al*: The mutational constraint spectrum quantified from variation in 141,456 humans. Nature 581: 434-443, 2020.
10. Sim NL, Kumar P, Hu J, Henikoff S, Schneider G and Ng PC: SIFT web server: Predicting effects of amino acid substitutions on proteins. Nucleic Acids Res 40 (Web Server Issue): W452-W457, 2012.
11. Adzhubei IA, Schmidt S, Peshkin L, Ramensky VE, Gerasimova A, Bork P, Kondrashov AS and Sunyaev SR: A method and server for predicting damaging missense mutations. Nat Methods 7: 248-249, 2010.
12. Steinhaus R, Proft S, Schuelke M, Cooper DN, Schwarz JM and Seelow D: MutationTaster2021. Nucleic Acids Re 49 (W1): W446-W451, 2021.
13. Rentzsch P, Witten D, Cooper GM, Shendure J and Kircher M: CADD: Predicting the deleteriousness of variants throughout the human genome. Nucleic Acids Res 47 (D1): D886-D894, 2019.
14. Ratnapriya R, Sosina OA, Starostik MR, Kwicklis M, Kapphahn RJ, Fritsche LG, Walton A, Arvanitis M, Gieser L, Pietraszkiewicz A, *et al*: Retinal transcriptome and eQTL analyses identify genes associated with age-related macular degeneration. Nat Genet 51: 606-610, 2019.
15. Yao Y, Fu J, Li L, Chen W, Meng Z, Su H and Dai W: Retinal and circumpapillary nerve fiber layer thickness and associated factors in children. Eye (Lond) 35: 2802-2811, 2021.
16. Hansen MC, Haferlach T and Nyvold CG: A decade with whole exome sequencing in haematology. Br J Haematol 188: 367-382, 2020.
17. Kaupp UB and Seifert R: Cyclic nucleotide-gated ion channels. Physiol Rev 82: 769-824, 2002.
18. Hornbeck PV, Zhang B, Murray B, Kornhauser JM, Latham V and Skrzypek E: PhosphoSitePlus, 2014: Mutations, PTMs and recalibrations. Nucleic Acids Res 43(Database Issue): D512-D520, 2015.
19. Hardman G, Perkins S, Brownridge PJ, Clarke CJ, Byrne DP, Campbell AE, Kalyuzhnyy A, Myall A, Eyers PA, Jones AR and Eyers CE: Strong anion exchange-mediated phosphoproteomics reveals extensive human non-canonical phosphorylation. EMBO J 38: e100847, 2019.
20. Zhang Y, He X, Zou J, Yang J, Ma A and Tan M: Phosphorylation mutation impairs the promoting effect of spastin on neurite outgrowth without affecting its microtubule severing ability. Eur J Histochem 67: 3594, 2023.
21. Kaushik S and Cuervo AM: AMPK-dependent phosphorylation of lipid droplet protein PLIN2 triggers its degradation by CMA. Autophagy 12: 432-438, 2016.
22. Michaelides M, Hunt DM and Moore AT: The cone dysfunction syndromes. Br J Ophthalmol 88: 291-297, 2004.
23. Michaelides M, Hardcastle AJ, Hunt DM and Moore AT: Progressive cone and cone-rod dystrophies: Phenotypes and underlying molecular genetic basis. Surv Ophthalmol 51: 232-258, 2006.
24. Michaelides M, Aligianis IA, Ainsworth JR, Good P, Mollon JD, Maher ER, Moore AT and Hunt DM: Progressive cone dystrophy associated with mutation in CNGB3. Invest Ophthalmol Vis Sci 45: 1975-1982, 2004.
25. Wycisk KA, Zeitz C, Feil S, Wittmer M, Forster U, Neidhardt J, Wissinger B, Zrenner E, Wilke R, Kohl S and Berger W: Mutation in the auxiliary calcium-channel subunit CACNA2D4 causes autosomal recessive cone dystrophy. Am J Hum Genet 79: 973-977, 2006.
26. Fujinami K, Zernant J, Chana RK, Wright GA, Tsunoda K, Ozawa Y, Tsubota K, Robson AG, Holder GE, Allikmets R, *et al*: Clinical and molecular characteristics of childhood-onset Stargardt disease. Ophthalmology 122: 326-334, 2015.
27. Xu K, Xie Y, Sun T, Zhang X, Chen C and Li Y: Genetic and clinical findings in a Chinese cohort with Leber congenital amaurosis and early onset severe retinal dystrophy. Br J Ophthalmol 104: 932-937, 2020.
28. Wissinger B, Gamer D, Jägle H, Giorda R, Marx T, Mayer S, Tippmann S, Broghammer M, Jurklies B, Rosenberg T, *et al*: CNGA3 mutations in hereditary cone photoreceptor disorders. Am J Hum Genet 69: 722-737, 2001.
29. Huang L, Xiao X, Li S, Jia X, Wang P, Sun W, Xu Y, Xin W, Guo X and Zhang Q: Molecular genetics of cone-rod dystrophy in Chinese patients: New data from 61 probands and mutation overview of 163 probands. Exp Eye Res 146: 252-258, 2016.
30. Kuniyoshi K, Muraki-Oda S, Ueyama H, Toyoda F, Sakuramoto H, Ogita H, Irifune M, Yamamoto S, Nakao A, Tsunoda K, *et al*: Novel mutations in the gene for α-subunit of retinal cone cyclic nucleotide-gated channels in a Japanese patient with congenital achromatopsia. Jpn J Ophthalmol 60: 187-197, 2016.
31. Thiadens AAHJ, Roosing S, Collin RWJ, van Moll-Ramirez N, van Lith-Verhoeven JJC, van Schooneveld MJ, den Hollander AI, van den Born LI, Hoyng CB, Cremers FPM and Klaver CCW: Comprehensive analysis of the achromatopsia genes CNGA3 and CNGB3 in progressive cone dystrophy. Ophthalmology 117: 825-830.e1, 2010.
32. Li S, Huang L, Xiao X, Jia X, Guo X and Zhang Q: Identification of CNGA3 mutations in 46 families: Common cause of achromatopsia and cone-rod dystrophies in Chinese patients. JAMA Ophthalmol 132: 1076-1083, 2014.
33. Saqib MA, Nikopoulos K, Ullah E, Sher Khan F, Iqbal J, Bibi R, Jarral A, Sajid S, Nishiguchi KM, Venturini G, *et al*: Homozygosity mapping reveals novel and known mutations in Pakistani families with inherited retinal dystrophies. Sci Rep 5: 9965, 2015.
34. Liu C and Varnum MD: Functional consequences of progressive cone dystrophy-associated mutations in the human cone photoreceptor cyclic nucleotide-gated channel CNGA3 subunit. Am J Physiol Cell Physiol 289: C187-C198, 2005.
35. Muraki-Oda S, Toyoda F, Okada A, Tanabe S, Yamade S, Ueyama H, Matsuura H and Ohji M: Functional analysis of rod monochromacy-associated missense mutations in the CNGA3 subunit of the cone photoreceptor cGMP-gated channel. Biochem Biophys Res Commun 362: 88-93, 2007.
36. Zelinger L, Cideciyan AV, Kohl S, Schwartz SB, Rosenmann A, Eli D, Sumaroka A, Roman AJ, Luo X, Brown C, *et al*: Genetics and disease expression in the CNGA3 form of achromatopsia: Steps on the path to gene therapy. Ophthalmology 122: 997-1007, 2015.
37. Kohl S, Marx T, Giddings I, Jägle H, Jacobson SG, Apfelstedt-Sylla E, Zrenner E, Sharpe LT and Wissinger B: Total colourblindness is caused by mutations in the gene encoding the alpha-subunit of the cone photoreceptor cGMP-gated cation channel. Nat Genet 19: 257-259, 1998.
38. Nishiguchi KM, Sandberg MA, Gorji N, Berson EL and Dryja TP: Cone cGMP-gated channel mutations and clinical findings in patients with achromatopsia, macular degeneration, and other hereditary cone diseases. Hum Mutat 25: 248-258, 2005.
39. Koeppen K, Reuter P, Ladewig T, Kohl S, Baumann B, Jacobson SG, Plomp AS, Hamel CP, Janecke AR and Wissinger B: Dissecting the pathogenic mechanisms of mutations in the pore region of the human cone photoreceptor cyclic nucleotide-gated channel. Hum Mutat 31: 830-839, 2010.
40. Azam M, Collin RW, Shah ST, Shah AA, Khan MI, Hussain A, Sadeque A, Strom TM, Thiadens AA, Roosing S, *et al*: Novel CNGA3 and CNGB3 mutations in two Pakistani families with achromatopsia. Mol Vis 16: 774-781, 2010.
41. Thapa A, Morris L, Xu J, Ma H, Michalakis S, Biel M and Ding XQ: Endoplasmic reticulum stress-associated cone photoreceptor degeneration in cyclic nucleotide-gated channel deficiency. J Biol Chem 287: 18018-18029, 2012.
42. Paquet-Durand F, Beck S, Michalakis S, Goldmann T, Huber G, Mühlfriedel R, Trifunović D, Fischer MD, Fahl E, Duetsch G, *et al*: A key role for cyclic nucleotide gated (CNG) channels in cGMP-related retinitis pigmentosa. Hum Mol Genet 20: 941-947, 2011.

43. Xu J, Morris L, Thapa A, Ma H, Michalakis S, Biel M, Baehr W, Peshenko IV, Dizhoor AM and Ding XQ: cGMP accumulation causes photoreceptor degeneration in CNG channel deficiency: Evidence of cGMP cytotoxicity independently of enhanced CNG channel function. J Neurosci 33: 14939-14948, 2013.
44. Yau KW: Cyclic nucleotide-gated channels: An expanding new family of ion channels. Proc Natl Acad Sci USA 91: 3481-3483, 1994.
45. Nakamura T and Gold GH: A cyclic nucleotide-gated conductance in olfactory receptor cilia. Nature 325: 442-444, 1987.
46. Tanaka JC, Eccleston JF and Furman RE: Photoreceptor channel activation by nucleotide derivatives. Biochemistry 28: 2776-2784, 1989.
47. Sundin OH, Yang JM, Li Y, Zhu D, Hurd JN, Mitchell TN, Silva ED and Maumenee IH: Genetic basis of total colourblindness among the Pingelapese islanders. Nat Genet 25: 289-293, 2000.
48. Georgiou M, Fujinami K and Michaelides M: Retinal imaging in inherited retinal diseases. Ann Eye Sci 5: 25, 2020.
49. Lima LH, Sallum JMF and Spaide RF: Outer retina analysis by optical coherence tomography in cone-rod dystrophy patients. Retina 33: 1877-1880, 2013.
50. Cho SC, Woo SJ, Park KH and Hwang JM: Morphologic characteristics of the outer retina in cone dystrophy on spectral-domain optical coherence tomography. Korean J Ophthalmol 27: 19-27, 2013.
51. Inui E, Oishi A, Oishi M, Ogino K, Makiyama Y, Gotoh N, Kurimoto M and Yoshimura N: Tomographic comparison of cone-rod and rod-cone retinal dystrophies. Graefes Arch Clin Exp Ophthalmol 252: 1065-1069, 2014.
52. Hamel CP: Cone rod dystrophies. Orphanet J Rare Dis 2: 7, 2007.
53. Sahel JA, Marazova K and Audo I: Clinical characteristics and current therapies for inherited retinal degenerations. Cold Spring Harb Perspect Med 5: a017111, 2014.
54. Prado DA, Acosta-Acero M and Maldonado RS: Gene therapy beyond luxturna: A new horizon of the treatment for inherited retinal disease. Curr Opin Ophthalmol 31: 147-154, 2020.
55. Maeder ML, Stefanidakis M, Wilson CJ, Baral R, Barrera LA, Bounoutas GS, Bumcrot D, Chao H, Ciulla DM, DaSilva JA, *et al*: Development of a gene-editing approach to restore vision loss in Leber congenital amaurosis type 10. Nat Med 25: 229-233, 2019.
56. Farrar GJ, Millington-Ward S, Chadderton N, Humphries P and Kenna PF: Gene-based therapies for dominantly inherited retinopathies. Gene Ther 19: 137-144, 2012.
57. Han Z, Conley SM, Makkia RS, Cooper MJ and Naash MI: DNA nanoparticle-mediated ABCA4 delivery rescues Stargardt dystrophy in mice. J Clin Invest 122: 3221-3226, 2012.
58. Sarra GM, Stephens C, de Alwis M, Bainbridge JW, Smith AJ, Thrasher AJ and Ali RR: Gene replacement therapy in the retinal degeneration slow (rds) mouse: The effect on retinal degeneration following partial transduction of the retina. Hum Mol Genet 10: 2353-2361, 2001.
59. Russell S, Bennett J, Wellman JA, Chung DC, Yu ZF, Tillman A, Wittes J, Pappas J, Elci O, McCague S, *et al*: Efficacy and safety of voretigene neparvovec (AAV2-hRPE65v2) in patients with RPE65-mediated inherited retinal dystrophy: A randomised, controlled, open-label, phase 3 trial. Lancet 390: 849-860, 2017.
60. Jiang L, Zhang H, Dizhoor AM, Boye SE, Hauswirth WW, Frederick JM and Baehr W: Long-term RNA interference gene therapy in a dominant retinitis pigmentosa mouse model. Proc Natl Acad Sci USA 108: 18476-18481, 2011.
61. Jiang L, Frederick JM and Baehr W: RNA interference gene therapy in dominant retinitis pigmentosa and cone-rod dystrophy mouse models caused by GCAP1 mutations. Front Mol Neurosci 7: 25, 2014.
62. Jiang L, Li TZ, Boye SE, Hauswirth WW, Frederick JM and Baehr W: RNAi-mediated gene suppression in a GCAP1(L151F) cone-rod dystrophy mouse model. PLoS One 8: e57676, 2013.
63. Ortín-Martínez A, Valiente-Soriano FJ, García-Ayuso D, Alarcón-Martínez L, Jiménez-López M, Bernal-Garro JM, Nieto-López L, Nadal-Nicolás FM, Villegas-Pérez MP, Wheeler LA and Vidal-Sanz M: A novel in vivo model of focal light emitting diode-induced cone-photoreceptor phototoxicity: neuroprotection afforded by brimonidine, BDNF, PEDF or bFGF. PLoS One 9: e113798, 2014.
64. Punzo C, Kornacker K and Cepko CL: Stimulation of the insulin/mTOR pathway delays cone death in a mouse model of retinitis pigmentosa. Nat Neurosci 12: 44-52, 2009.
65. Aït-Ali N, Fridlich R, Millet-Puel G, Clérin E, Delalande F, Jaillard C, Blond F, Perrocheau L, Reichman S, Byrne LC, *et al*: Rod-derived cone viability factor promotes cone survival by stimulating aerobic glycolysis. Cell 161: 817-832, 2015.
66. Yang Y, Mohand-Said S, Danan A, Simonutti M, Fontaine V, Clerin E, Picaud S, Léveillard T and Sahel JA: Functional cone rescue by RdCVF protein in a dominant model of retinitis pigmentosa. Mol Ther 17: 787-795, 2009.
67. Johnson S, Michaelides M, Aligianis IA, Ainsworth JR, Mollon JD, Maher ER, Moore AT and Hunt DM: Achromatopsia caused by novel mutations in both CNGA3 and CNGB3. J Med Genet 41: e20, 2004.
68. Ellingford JM, Barton S, Bhaskar S, O'Sullivan J, Williams SG, Lamb JA, Panda B, Sergouniotis PI, Gillespie RL, Daiger SP, *et al*: Molecular findings from 537 individuals with inherited retinal disease. J Med Genet 53: 761-767, 2016.
69. Reuter P, Koeppen K, Ladewig T, Kohl S, Baumann B and Wissinger B; Achromatopsia Clinical Study Group: Mutations in CNGA3 impair trafficking or function of cone cyclic nucleotide-gated channels, resulting in achromatopsia. Hum Mutat 29: 1228-1236, 2008.
70. Carss KJ, Arno G, Erwood M, Stephens J, Sanchis-Juan A, Hull S, Megy K, Grozeva D, Dewhurst E, Malka S, *et al*: Comprehensive rare variant analysis via whole-genome sequencing to determine the molecular pathology of inherited retinal disease. Am J Hum Genet 100: 75-90, 2017.